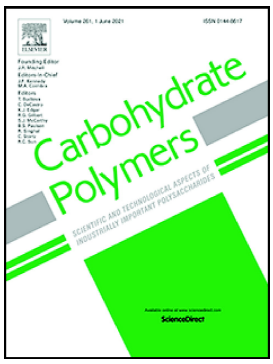

Thiolated α-cyclodextrin: The likely smallest drug carrier providing enhanced cellular uptake and endosomal escape

Özlem Kaplan, Martyna Truszkowska, Gergely Kali, Patrick Knoll, Mariana Blanco Massani, Doris Elfriede Braun, Andreas Bernkop-Schnürch

PII: S0144-8617(23)00535-0

DOI: https://doi.org/10.1016/j.carbpol.2023.121070

Reference: CARP 121070

To appear in: *Carbohydrate Polymers*

Please cite this article as: Ö. Kaplan, M. Truszkowska, G. Kali, et al., Thiolated α-cyclodextrin: The likely smallest drug carrier providing enhanced cellular uptake and endosomal escape, *Carbohydrate Polymers* (2023), https://doi.org/10.1016/j.carbpol.2023.121070

Thiolated α-Cyclodextrin: The Likely Smallest Drug Carrier Providing Enhanced Cellular Uptake and Endosomal Escape

Graphical abstract

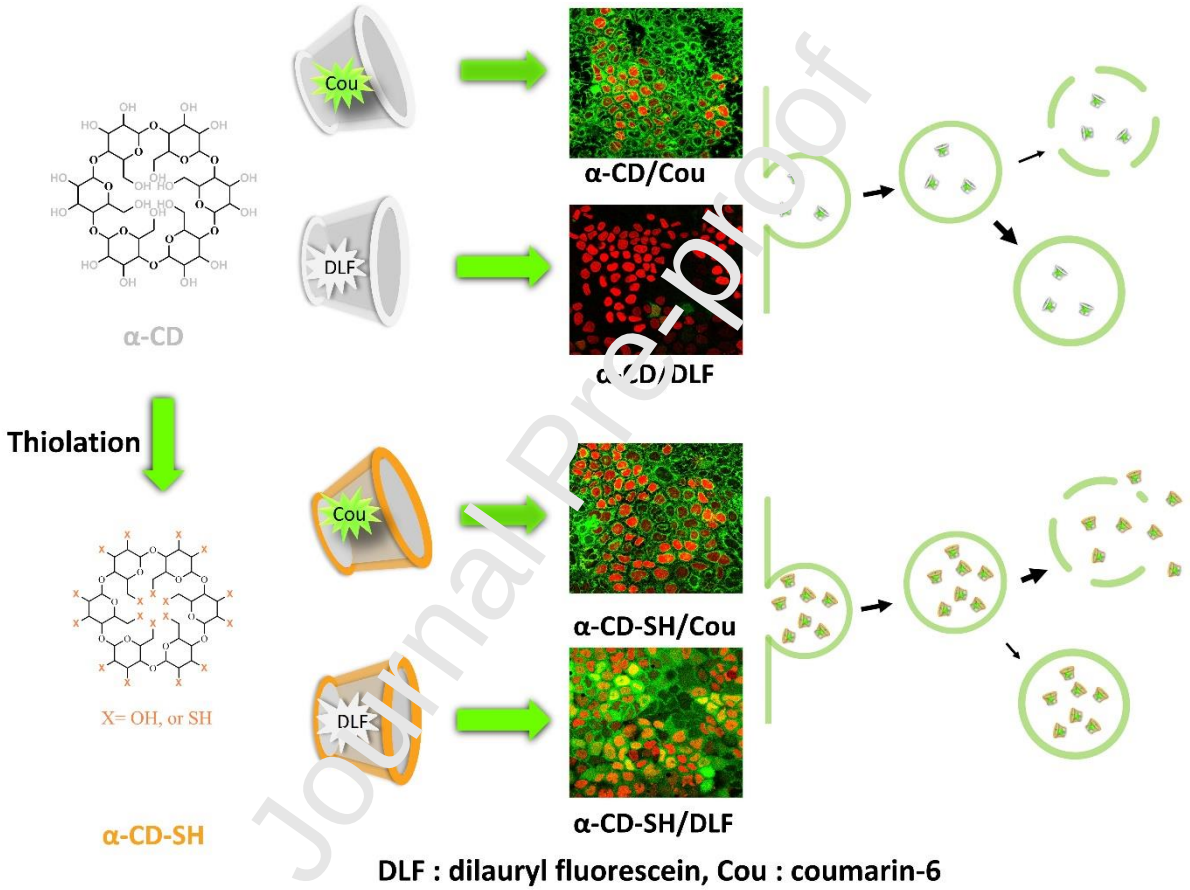

Thiolated α-Cyclodextrin: The Likely Smallest Drug Carrier Providing Enhanced Cellular Uptake and Endosomal Escape

Özlem Kaplan [a, b], Martyna Truszkowska [c], Gergely Kali [c], Patrick Knoll [c], Mariana Blanco Massani [c], Doris Elfriede Braun [c], Andreas Bernkop-Schnürch [c] *

[a] Department of Genetics and Bioengineering, Rafet Kayış Faculty of Engineering, Alanya Alaaddin Keykubat University, 07400, Antalya, Turkey

[b] Department of Molecular Biology and Genetics, Faculty of Science, Istanbul University, 34134, Istanbul, Turkey

[c] Center for Chemistry and Biomedicine, Department of Pharmaceutical Technology, Institute of Pharmacy, University of Innsbruck, Innrain 80-82, A-6020 Innsbruck, Austria

*Corresponding author

Andreas Bernkop-Schnürch

E-mail address: andreas.bernkop@uibk.ac.at

ABSTRACT

This study aimed to evaluate the effect of thiolated α-cyclodextrin (α-CD-SH) on the cellular uptake of its payload.

For this purpose, α-CD was thiolated using phosphorous pentasulfide. Thiolated α-CD was characterized by FT-IR and ^{1}H NMR spectroscopy, differential scanning calorimetry (DSC), and powder X-ray diffractometry (PXRD). Cytotoxicity of α-CD-SH was evaluated on Caco-2, HEK 293, and MC3T3 cells. Dilauryl fluorescein (DLF) and coumarin-6 (Cou) serving as surrogates for a pharmaceutical payload were incorporated in α-CD-SH, and cellular uptake was analyzed by flow cytometry and confocal microscopy. Endosomal escape was investigated by confocal microscopy and hemolysis assay.

Results showed no cytotoxic effect within 3 h, while dose-dependent cytotoxicity was observed within 24 h. The cellular uptake of DLF and Cou was up to 20- and 11-fold enhanced by α-CD-SH compared to native α-CD, respectively. Furthermore, α-CD-SH provided an endosomal escape.

According to these results, α-CD-SH is a promising carrier to shuttle drugs into the cytoplasm of target cells.

Keywords: cyclodextrin, thiolated cyclodextrin, endosomal escape, cellular uptake, thiol-mediated cellular uptake

1. INTRODUCTION

Cyclodextrins (CDs) have been extensively investigated as pharmaceutical excipients in order to increase the solubility and chemical stability of small molecular drugs through host-guest interactions (Jacob & Nair, 2018; Sahoo et al., 2021). Because of these beneficial properties, they are used in numerous drug delivery systems such as oral (Li et al., 2022), nasal (Mirankó, Tóth, Bartos, Ambrus, & Feczkó, 2023), ocular (Asim et al., 2021; Q. Wang et al., 2023), dermal (Oktay, Celebi, Ilbasmis-Tamer, & Kaplanoğlu, 2023), rectal (Lázaro et al., 2020; L.-L. Wang, Zheng, Chen, Han, & Jiang, 2016), sublingual (Londhe & Shirsat, 2018; Topuz, 2022) and parenteral (Gérard Yaméogo et al., 2020).

Shortcomings of CDs, such as, in some cases, poor aqueous solubility or short gastrointestinal residence time, can be addressed by the design of derivatives. The covalent attachment of hydroxypropyl and sulfobutyl groups to CDs leads to highly soluble derivatives (Poulson et al., 2022). Among CD derivatives, thiolated CDs moved into the limelight of research more recently (Asim, Ijaz, Rösch, & Bernkop-Schnürch, 2020; Grassiri, Cesari, et al., 2022; Grassiri, Knoll, et al., 2022). Since thiolated CDs are able to form disulfide bonds with cysteine-rich subdomains of mucus glycoproteins, they exhibit high mucoadhesive properties, substantially prolonging the mucosal residence time of numerous drugs. Grassiri et al. showed a 4-fold increased concentration of dexamethasone in the aqueous humour of rabbits due to a significantly prolonged ocular residence time of this drug provided by thiolated hydroxypropyl-β-CD versus the corresponding unmodified CD (Grassiri, Knoll, et al., 2022). Introducing thiol groups might even lead to other beneficial properties of CDs as well. In particular, cellular uptake-enhancing properties could be gained by thiolation, as thiol groups naturally present on the cell surface are known to enhance cellular association and internalization of various materials bearing thiol-reactive groups in their structure (Torres & Gait, 2012). The transfection efficacy of chitosan/pDNA nanoparticles was 2.5-fold enhanced when using thiolated chitosan

instead of the unmodified polysaccharide in these nanocarriers (Loretz, Thaler, & Bernkop-Schnürch, 2007). So far, however, the impact of thiol groups in the structure of CDs on their cellular uptake has not been investigated. We hypothesize that thiolated CDs enhance cellular uptake.

It was, therefore, the aim of this study to evaluate the cellular uptake of a thiolated CD. To that end, the smallest available CD (α-CD) was thiolated (α-CD-SH) according to a method recently developed by our research group (Kali, Haddadzadegan, Laffleur, & Bernkop-Schnürch, 2023) and characterized by FT-IR, ^{1}H NMR, XRD, and DSC. Cytotoxicity of α-CD-SH was evaluated on Caco-2, HEK 293, and MC3T3 cells. Dilauryl fluorescein (DLF) and coumarin-6 were chosen because of their fluorescence as surrogates for a pharmaceutical payload and incorporated in α-CD-SH to probe its drug-transporting potential. Cellular uptake was analyzed by flow cytometry and confocal microscopy. Based on the latter, we generated the new hypothesis that and endosomal escape could be promoted by thiolation. This was investigated via a hemolysis assay and confocal microscopy.

2. MATERIALS AND METHODS

2.1. Materials

Phosphorus pentasulfide, tetramethylene sulfone, dimethyl sulfoxide- d6, 7-hydroxy-3H-phenoxazin-3-one-10-oxide sodium salt (Alamar Blue, Resazurin sodium salt), L-cysteine hydrochloride, coumarin-6 and dilauryl fluorescein were ordered from Sigma-Aldrich, Austria. Alpha cyclodextrin (α-CD) was purchased from Cyclolab, Hungary. 5,5′-Dithiobis(2-nitrobenzoic acid) (Ellman's reagent) and Triton^{TM} X-100 were obtained from Merck, Germany. NucSpot Live 650 was ordered from Biotum, America. Minimum essential eagle medium (MEM), alpha MEM and OptiMEM were obtained from ThermoFisher Scientific, Austria.

2.2. Synthesis of α-CD-SH

α-CD was thiolated according to a method described previously for β-CD with some modifications (Kali et al., 2023). First, α-CD (1 g, 1.02 mmol) and phosphorus pentasulfide (4.8 g, 21.5 mmol) were dissolved in 30 mL of sulfolane. Triethylamine (2 mL, 14.3 mmol) was added to the solution. The mixture was heated to 150 °C and stirred for one hour. At the end of the incubation period, the temperature was decreased to 50°C, and distilled water was added to remove the remaining P_2S_5. The product was dialyzed for four days in the dark at 10°C and pH~6 using Spectra/Pore dialysis membrane (MWCO: 1000 Da) and then lyophilized.

2.3. Characterization of α-CD-SH

^{1}H and ^{13}C NMR measurements of α-CD-SH were performed in dimethyl sulfoxide-d6 (DMSO-d6) solution using a "Mars" 400 MHz Avance 4 Neo spectrometer from Bruker Corporation (Billerica, MA, USA, 400 MHz). FTIR measurements of α-CD-SH were performed using Bruker ALPHA FT-IR instrument.

The free thiol content of α-CD-SH was determined by the Ellman's test (Ijaz et al., 2015). Briefly, modified α-CD was dissolved in Ellman's buffer, and Ellman's reagent (5,5'-dithiobis (2-nitrobenzoic)) was added to the sample. After 90 min incubation at room temperature, the absorbance value at 450 nm was recorded using Tecan Spark microplate reader (M-200 spectrometer, Tecan, Grödig, Austria). The amount of free thiol groups of α-CD-SH was calculated using L-cysteine as a standard for the calibration curve. Disulfide bridges were quantified using Ellman's test after reducing the disulfide bonds in the product with sodium borohydride ($NaBH_4$) (Laquintana et al., 2019).

To determine the water solubility, 5 mg of α-CD-SH was added to 100 µL of distilled water, and the sample was incubated under agitation (1200 rpm) at 25 °C and 37 °C for 24 h.

Undissolved α-CD-SH was removed by centrifugation at 13 400 rpm for 10 minutes, the supernatant was lyophilized, and α-CD-SH was gravimetrically quantified (Kali et al., 2023).

pKa of α-CD-SH was determined by measuring UV absorption at stepwise raised pH values (Asim, Nazir, Jalil, Laffleur, et al., 2020). Briefly, α-CD-SH (0.5% m/v) was dissolved in 100 mM NaCl containing 1 mM HCl, and the pH of the solution was adjusted to different values using 0.01% NaOH. The absorbance at 242 nm at different pH values was measured. The term -log $(Amax - Ai)\ /Ai$ as a function of pH was used to calculate pKa. (Amax: absorbance of completely deprotonated thiols at high pH Ai: Absorbance of thiols at different pH values)

2.4. Cytotoxicity Studies

Cytotoxicity of native and thiolated α-CD on Caco-2 (human colorectal adenocarcinoma cells), HEK 293 (Human embryonic kidney), and MC3T3-E1 subclone 4 (MC3T3, commercial murine calvaria pre-osteoblast cell line -ATCC CRL2593) cells were determined via resazurin assay (Veider, Akkuş-Dağdeviren, Knoll, & Bernkop-Schnürch, 2022). For this test, 96 well plates with a seeding concentration of $2 X\ 10^5$ cells/well of Caco-2 and HEK 293 cells were grown in MEM, while for MC3T3, $2 X\ 10^4$ cells/well were seeded and grown in α-MEM (Fisher Scientific) (Gong et al., 2020). Cells were incubated at 37 °C under 5 % CO_2 and 95 % relative humidity until confluency was reached. Three concentrations (0.5, 1, and 5 mg/mL) of native and thiolated α-CD dissolved in HEPES buffer (pH:7.4) were applied to cells. The growing medium without phenol red was used as a positive control, and 0.1% v/v Triton^{TM} X-100 was used as a negative control. After 3 h and 24 h incubation, test solutions were removed, and cells were washed twice with buffer. Resazurin solution (Sigma-Aldrich) was applied to each well and incubated for 3 hours at 37°C under 5 % CO_2 and 95 % relative humidity environment. The fluorescence of the supernatant was measured (λ_{Ex} 540 nm, λ_{Em} 590 nm) using Tecan Spark microplate reader. Cell viability was calculated using the following formula, and the data were normalized for the buffer effect.

$$\text{Cell viability (\%)} = \frac{\text{Sample} - \text{Negative control}}{\text{Positive control} - \text{Negative control}} X100$$

2.5. Determination of Hemolysis Activity

Since the cellular membrane of erythrocytes is susceptible and fragile, the hemolysis activity assay allows detailed conclusions about membrane damage and cell toxicity (Evans et al., 2013). Additionally, the cellular membrane of red blood cells (RBC) is frequently used to mimic the *in vivo* conditions after endosomal internalization. Hemolysis activity was determined spectroscopically, as previously described by Friedl et al. (2020). Briefly, human blood sample kindly supplied by Tirol Kliniken GmbH (Innsbruck, Austria) was diluted (1:200 volume ratio) in sterile HEPES buffer. Test solutions containing native and thiolated α-CDs with three different concentrations (0.125 mg/mL, 0.25 mg/mL, and 0.5 mg/mL) in HEPES buffer (pH 7.4) were added to the RBC suspension (1:1 volume ratio) and incubated on thermomixer (Eppendorf) at 37°C with agitation (300 rpm) for 3 h and 24 h. Triton X-100 (1% v/v) was used as a positive control (100 % reference value for hemolysis). Afterward, the samples were centrifuged at 2700 rpm for 10 minutes, and the absorbance values of the supernatant were determined at a wavelength of 415 nm (Friedl, Steinbring, Zaichik, Le, & Bernkop-Schnürch, 2020).

The percentage of hemolysis was calculated with the following formula:

$$\text{Hemolysis (\%)} = \frac{\text{A(sample)} - \text{A(buffer)}}{\text{A(Triton X} - 100) - \text{A(buffer)}}$$

2.6. Fluorescent Labeling of α-CDs

Fluorescent labeling of α-CDs was performed as previously reported by our group using dilauryl fluorescein (DLF) and coumarin-6 (Cou) dyes (Asim et al., 2018; Asim, Nazir, Jalil, Matuszczak, & Bernkop-Schnürch, 2020; Grassiri, Knoll, et al., 2022; Kali et al., 2023). Based on some previous studies, α-CDs are not forming real inclusion complex with Cou, but they

accumulate around the Cou micro aggregates (Ghosh, Das, Maity, Mondal, & Purkayastha, 2015). Firstly, 30 mg of thiolated and native α-CDs were suspended in 30 mL of demineralized water, and the pH was adjusted to 6.5. Then, 1 mL of two ethanolic dye solutions, 0.02% (m/v) DLF (molar ratio to CD 100:1) and 0.02% (m/v) Cou (molar ratio to CD 5:1), were separately added to α-CDs aqueous solutions and stirred at room temperature for 24 h. After that, the suspensions were filtered to remove free dye and lyophilized.

2.7. Thermal Analysis

2.7.1. Thermomicroscopic characterization

DLF, Cou, thiolated and native α-CD were investigated with a BH2 polarizing microscope (Olympus, A) equipped with a Koffler hot-stage (Reichert, Austria) and an Olympus DP71 digital camera. The solid CDs were analyzed in cross-polarized light.

2.7.2. Differential Scanning Calorimetry

DSC thermograms were obtained with a DSC 7 (Perkin-Elmer, Norwalk, Ct, USA) using the Pyris 7. 0 software. Accordingly, 1-2 mg of samples (using a UM3 ultramicrobalance, Mettler, Greifensee, Switzerland) were weighed into one-pin hole aluminum capsules. The samples were heated using a rate of 10 °C min^{-1} with dry nitrogen. The instrument was calibrated for temperature with pure benzophenone (mp. 48.0 °C) and caffeine (236.0 °C), and the calibration of the energy was accomplished with indium (mp. 156.6 °C, the heat of fusion 28.45 J/g^{-1})

2.8. Powder X-Ray Diffraction

The powder x-ray diffraction (PXRD) patterns for characterizing DLF, Cou, α-CD and α-CD-SH were obtained using an X'Pert PRO diffractometer (PANalytical, Almelo, NL) equipped with a θ/θ coupled goniometer in transmission geometry, programmable XYZ stage with well plate holder, Cu $K_{a1,2}$ radiation source with a focusing mirror, a 0.5° divergence slit and a 0.02° Soller slit collimator and a solid-state PIXcel detector. The patterns were registered at a tube

voltage of 40 kV and tube current of 40 mA, applying a step size of 2θ = 0.013° with 200 or 400s per step in the 2θ range between 2° and 40°.

2.9. Cellular Uptake Studies

2.9.1. Flow Cytometry

Cells were seeded in a 24-well plate and incubated for two weeks at 37°C under 5 % CO_2 and 95 % relative humidity. Fluorescently labeled native and thiolated α-CD samples (0.05% m/v) dissolved in HEPES buffer and α-MEM without phenol red were applied to the Caco-2, HEK 293, and MC3T3 cells, respectively. After 3 hours of incubation at 4°C or 37°C, the cells were detached from the wells using trypsin (Merck KGaA, Darmstadt, Germany) and washed three times with ice-cold phosphate-buffered saline (PBS) (Merck KGaA, Darmstadt, Germany). All samples were analyzed by flow cytometry (Attune NxT Flow cytometer, Thermo Fisher Scientific, MA, USA). Trypan blue (Thermo Fischer Scientific) was applied in order to quench the fluorescence of non-intracellular surface-absorbed CDs (Srivastava et al., 2011). The relative mean fluorescence intensity values (RMFI) were calculated from the mean fluorescence intensity values (MFI) using the following formula (Friedl et al., 2020):

$$RMFI = \frac{\text{MFI of sample}}{\text{MFI of control}} - 1$$

2.9.2. Confocal Microscopy

Internalization of α-CDs by cells was further confirmed using confocal laser scanning microscopy (Leica TCS SP8) with appropriate filter sets. Briefly, cells were seeded in an eight-well chamber (μ-slide, Ibidi) in a density of 1 x 10^5 cells/ml (3 x 10^4 cells/well). After reaching confluence, cells were incubated with 0.05% of all labeled native and thiolated CDs dissolved in opti-MEM or α-white MEM (MC3T3) for 3 hours. The cells were then washed three times with prewarmed opti-MEM. The cell nuclei were stained using NucSpot Live 650 according to

the provider's recommendations (1µl of NucSpot Live 650 1000X in DMSO diluted in 1ml of OptiMEM) for 2 hours. However, since the dye was not toxic to the cells, the washing step after staining was not necessary. All fluorescence images were recorded under equivalent requirements. Image postprocessing was performed by ImageJ software: the yz- and xz-projections were performed from 5 XY images of an image stack at 0.2 µm z-step length. Spectral unmixing was applied to eliminate fluorescence bleed between detection channels due to overlapping emission spectra. Furthermore, 2D image filtering was regulated by using a Gaussian filter.

2.10. Statistical Analysis

All experiments were performed at least three times. GraphPad Prism 5 (GraphPad Software, Inc., San Diego, CA, USA) was used to analyze the data. The one-way ANOVA and two-way Bonferroni multiple comparison test was applied, and statistical significance was defined as $p<0.05$ probability values.

3. RESULTS AND DISCUSSION

3.1. Synthesis and Characterization of α-CD-SH

In this study, phosphorus pentasulfide in the presence of sulfolane and triethylamine was used for the thiolation of α-CD. The synthetic pathway is shown in **Figure 1**. The chemical structure of the α-CD-SH was confirmed by ^{1}H NMR and FT-IR analysis.

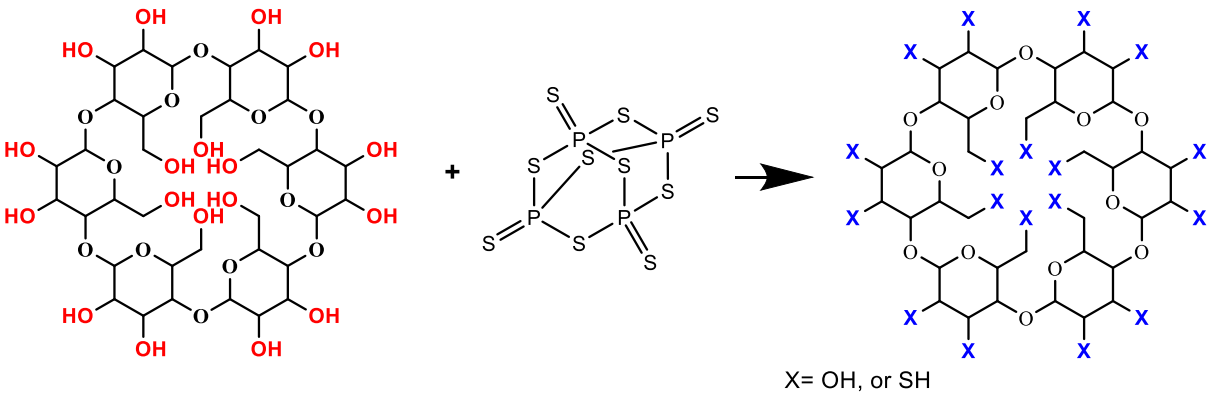

Figure 1. Schematic representation of the thiolation reaction of α-CD with phosphorus pentasulfide

The ^{1}H NMR spectrum of the product, recorded in DMSO-d_6 (**Figure S1a**), showed reduced chemical shifts for the OH groups at positions C-2 and C-3 at 5.60-5.30 ppm and position C-6 at 4.50-4.40 ppm. Furthermore, new peaks appeared for the sulfhydryl groups at positions 2.05 and 1.15 ppm, for positions C-2 and C-3, as well as for C-6, respectively. Based on the integral values of the anomeric proton and the remaining hydroxyls, the degree of modification is around 30%. NMR studies were made on freshly prepared thiolated α-CD in every purification step. The cross-peaks in the COSY spectrum of the product between the sulfhydryl groups and the H-3 - H-6 protons of CD also confirm the successful thiolation. **Figure S1** shows the spectrum of the thiolated CD before the last purification, including solvent peaks, as afterward, due to the water absorption and the hydrogen bonding with the remaining hydroxyl groups, the peaks cannot be separately integrated. No significant difference in the ^{1}H NMR spectrum of fresh and old samples was found, referring to sufficient product stability. Due to the thiol hydroxyl exchange, the 13C NMR spectrum of thiolated α-CD show slightly shifted peaks for C-2, C-3, and C-6. Thiolation of α-CD was also confirmed with Fourier transform infrared (FT-IR) spectroscopy showing a weak peak that can be assigned to -S-H stretching (~2660 cm^{-1}), together with a broad shoulder observed around 2333 cm^{-1} (Colthup, Daly, & Wiberley, 1990) (**Figure S2**). The PXRD measurements confirmed that α-CD is present in hexahydrate form (Manor & Saenger, 1974) (**Figure S3**). The PXRD pattern of α-CD-SH showed that a different crystal structure is obtained upon thiolation, albeit the material exhibited a low crystallinity, as indicated by the low Bragg reflection intensities and the broad 'halo'. The latter is not surprising, as the synthesis comprised a final lyophilization step. The DSC thermogram (**Figure S4**) of the native α-CD exhibited a broad endotherm at temperatures below 150 °C, originating from water loss. Dehydration was accompanied by a structural collapse, i.e., the amorphous

material was present at temperatures higher than 150 °C. From 275 °C onwards, applying a heating rate of 10 °C min^{-1}, decomposition of the α-CD occurred. The observations were additionally confirmed with hot-stage microscopy. In the case of α-CD-SH, the decomposition was seen at a slightly lower temperature than for α-CDs. Nevertheless, the α-CD-SH was thermally stable until above 200 °C (heating rate of 10 °C min^{-1}). As described for the α-CDs, loss of crystallinity could be observed for α-CD-SH upon heating in the temperature range from 105 to 130 °C.

Ellman's and disulfide bond tests were used to determine the amount of free thiol and disulfide substructures on α-CD-SH. The free thiol concentration was 327.83±213.46 µmol/g, while the disulfide bond concentration was 1376.09±43.13 µmol/g, that is 29.6% disulfide bond content for the product. Based on Ellman's and disulfide bond results, the degree of thiolation is about 32.69±1.62 %, which is in good agreement with the value calculated from the ^{1}H NMR spectrum.

The water solubility of α-CD-SH at 25 °C and 37 °C were 24.25 ± 0.29 mg/mL and 42.87 ± 0.46 mg/mL, respectively. This increase in solubility at higher temperature was previously shown for other CD derivatives (Jicsinszky, 2019). Compared to native α-CD, exhibiting a solubility of 145 mg/mL at 25 °C (Loftsson, Jarho, Másson, & Järvinen, 2005), at least 6-fold lower solubility of α-CD-SH was observed. The properties of modified CDs are mainly determined by the position of the modified hydroxyl groups on the CD (Syed Haroon, Mehreen, Sajid, Tauqeer Hussain, & Ikram Ullah, 2019). The decrease in solubility of α-CD-SH suggests that the remaining unmodified hydroxyl groups might form strong hydrogen bonding interactions. Moreover, this decrease in solubility of α-CD-SH might also be attributed to inter- and intramolecular disulfide bonds. This disulfide bond formation is highly dependent on the pKa of the thiol groups on α-CD-SH, providing information about the ratio of thiol to thiolate anions at certain pH values. Thiolate anions are reactive species responsible for a nucleophilic

attack on disulfide bonds, causing the thiol-disulfide exchange reactions. Figure 2A illustrates the UV absorption of the α-CD-SH at indicated pH values. As the pH of the α-CD-SH solution increases, the concentration of thiolate anions increases, which can be quantified by a raised absorbance. As shown in Figure 2A, plotting pH vs. absorbance revealed a strong increase in thiolate anions above pH 6. A range of pKa of α-CD-SH is estimated from Figure 2B between 6.5 and 7.7. Due to the scattering of the measured values, most probably because of the various thiols at C6, C3, and C2 positions, no single pKa could be determined, but the values are in this region, similar to that of a thiolated HP-β-CD described previously (Laquintana et al. 2019). At a physiological pH of 7.2, α-CD-SH is therefore highly reactive to form disulfide bonds with exofacial cellular membrane thiols via oxidation to disulfides via thiol/disulfide exchange reactions.

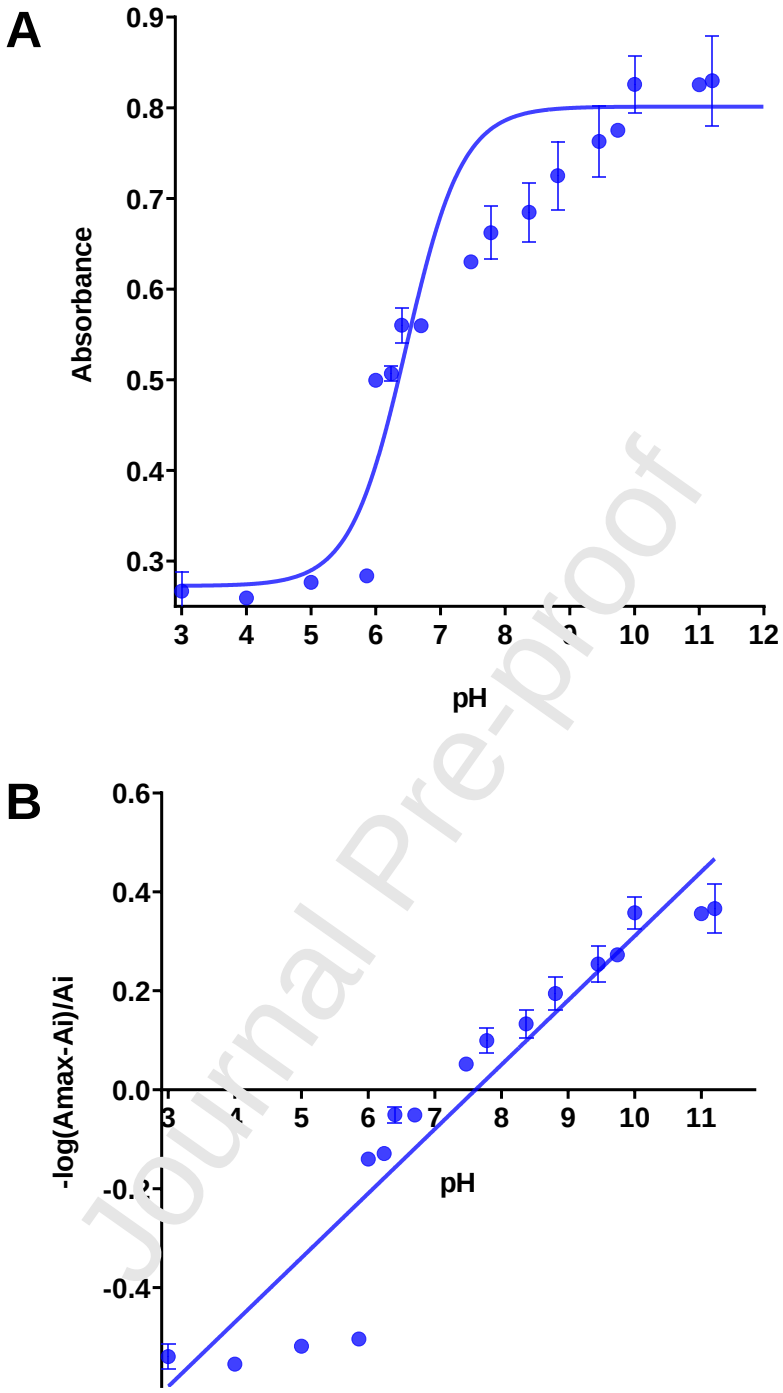

Figure 2. Determination of the pKa value by plotting the absorbance (A) of α-CD-SH as a function of pH and (B) −log [(Amax − Ai)/Ai] as a function of pH. Indicated values are means ± SD (n = 3)

3.2. Cytotoxicity Studies

The results of cytotoxicity studies of α-CD and α-CD-SH on Caco-2, HEK 293, and MC3T3 cells are shown in **Figure 3**. Native α-CD did not show any significant cytotoxic effect during 3 h and 24 h of incubation ($p<0.05$) at all concentrations applied to Caco-2 and MC3T3 cells (**Figure 3A, B, and 3E, F**, respectively), whereas at a concentration of 5 mg/mL, a significant ($p<0.05$) cytotoxic effect on HEK 293 was observed after 24 h of incubation (**Figure 3D**).

In contrast, α-CD-SH showed a cytotoxic effect at a concentration of 5 mg/mL within 3 h in the case of all tested cells (**Figure 3A, 3C, and 3E**). Merely on MC3T3 cells, a low toxic effect was observed for concentrations of 0.5 and 1 mg/mL (**Figure 3E**). Generally, α-CD-SH showed a time- and dose-dependent effect on all cells, leading to toxic effects from 1 mg/mL for Caco-2 (**Figure 3B**) and HEK cells (**Figure 3D**) and 0.5 mg/mL for MC3T3 (**Figure 3E**) after 24 h of incubation.

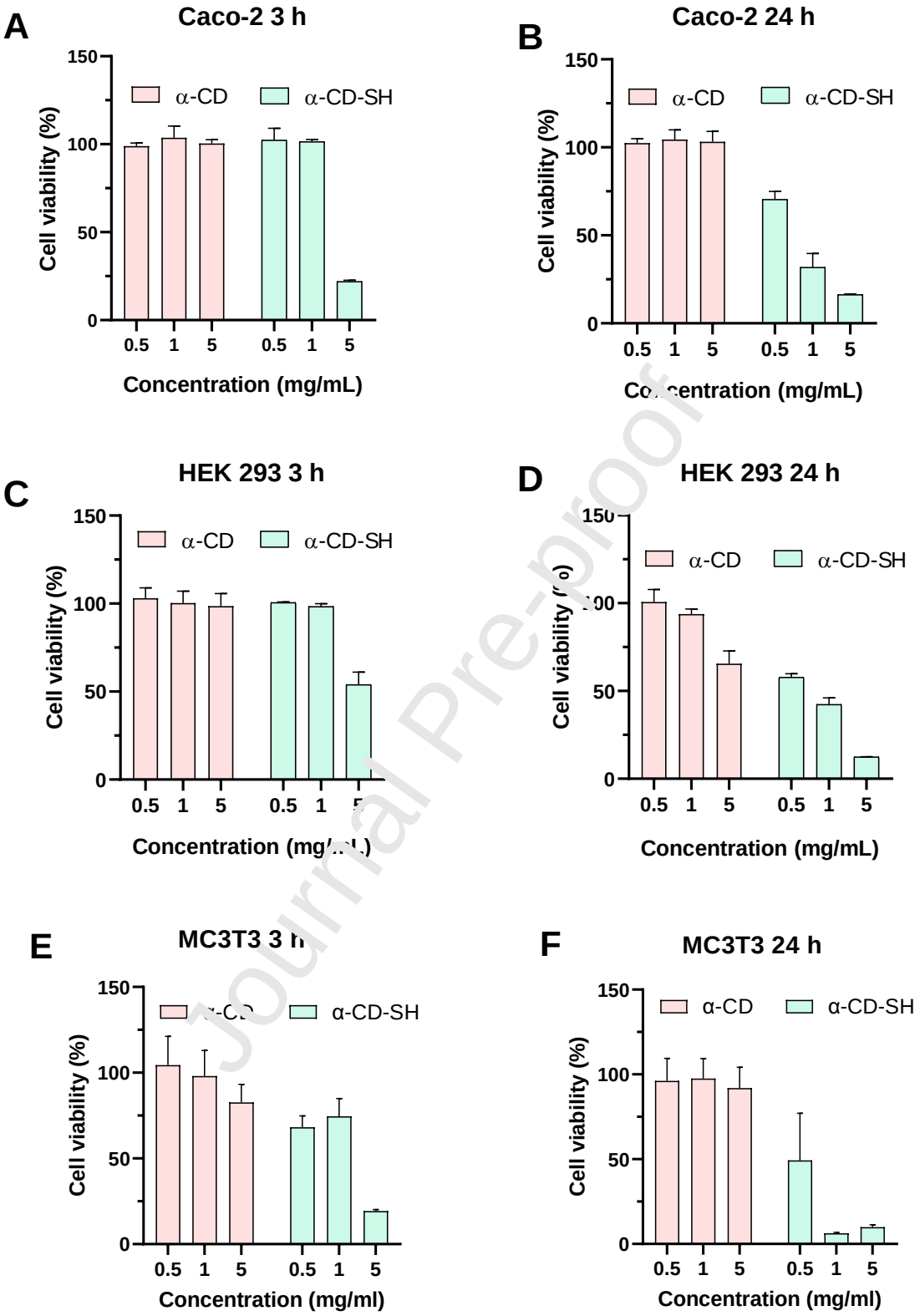

Figure 3. Cell viability of Caco-2 (A, B), HEK 293 (C, D), and MC3T3 (E, F) cells exposed to native and α-CD-SH for 3 h and 24 h. All results are shown as mean ± SD, n = 3.

3.3. Determination of Hemolysis Activity

Native CD showed minor hemolysis activity at all applied concentrations after 3 h, while α-CD-SH exhibited significant hemolysis activity at 0.25 and 0.5 mg/mL concentrations. The results of this study are illustrated in **Figure 4.**

The hemolysis potential of materials was previously correlated to their interaction with endosomal membranes. As our results showed significantly higher membrane interactions of α-CD-SH compared to α-CD, the potential of α-CD for endosomal escape seems to be enhanced by thiolation. Hemolysis experiments showed that α-CD-SH has a high endosomal escape potential. However, this also indicates its limited hemocompatibility. Therefore, α-CD-SH may need to be used in mucosal drug applications or by injecting directly into target tissues. In contrast to the α-CD-SH tested in this study, however. some thiolated CDs with high hemocompatibility have been reported in previous studies (Asim et al., 2021; Fürst et al., 2023).

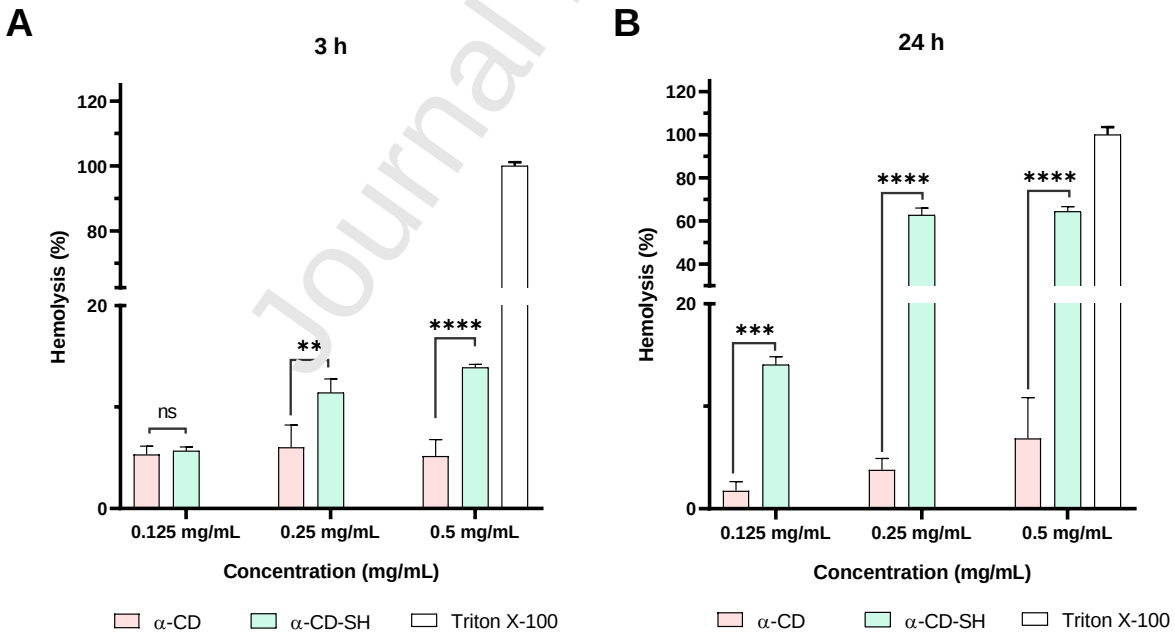

Figure 4. Hemolysis effect of native α-CD and while α-CD-SH on red blood cells after 3 h (A) and 24 h (B) of incubation at 37 °C. All results are shown as mean ± SD, n = 3. ns:not significant; ***p<0.005; *** p<0.0005; **** p<0.00005.*

Considering that α-CD-SH contains 1376 µmol/g disulfide bonds, the enhanced endosomal escape of this thiolated CD is in good agreement with previous studies. Kanjilal et al. have recently designed polymeric nanogels bearing disulfides at various positions that enabled endosomal escape, while without disulfide bounds, the polymeric nanogels did not show this result. Moreover, the exposure of disulfides on the outer surface of the nanogel further enhanced both cellular uptake and endosomal escape. The authors explained their observations by an endosomal escape mechanism based on thiol/disulfide exchange reactions between disulfide-bearing nanogels and membrane thiols, forcing the packaging of endosomal membranes and disrupting membrane integrity (Kanjilal, Dutta, & Thayumanavan, 2022). Endosomal escape is a major bottleneck in the design of delivery systems to transport therapeutic biomolecules into cells (Pei & Buyanova, 2019). Thiolated delivery systems might therefore be a promising approach to provide endosomal escape. In our system, disulfide bonds are already present, and above the pKa of the thiolated CDs, it is expected that disulfide bonds develop with time, which can be advantageous for cellular uptake and endosomal escape.

3.4. Cellular Uptake Studies

To compare the cellular uptake of native and thiolated α-CD complexes with the fluorescent molecules DLF and coumarin-6 were prepared. The complex formation was confirmed by ^{1}H NMR and PXRD. In the ^{1}H NMR spectra, some broad peaks of the fluorescent dyes could be detected in the region of 1.0-3.0 ppm for the methyl and methylene protons and small peaks at the aromatic region (7.5 – 8.0 ppm) (see Figure S5). In the PXRD diffractograms no peak positions of the fluorescent dyes were detectable (Figure S3).

The PXRD measurements of DLF and coumarin-6 revealed that the two compounds were crystalline. The absence of the DLF, coumarin-6 and α-CD peak positions in the PXRD patterns of the DLF and coumarin-6 complexes confirmed a structural rearrangement. The identical

PXRD characteristics of the two complexes indicate that the α-CD molecules adopt the same packing arrangement. A comparison of the experimental α-CD/Cou and α-CD/DLF PXRD diffractograms from known crystal structures (Taylor & Wood, 2019) simulated PXRD patterns suggests that the two α-CD complexes may be structurally related to the α-CD succinic acid clathrate hydrate (Saouane & Fabbiani, 2016), an inclusion complex. The PXRD pattern of the α-CD-SH modified with the fluorescent molecules resulted in amorphous materials, as additionally confirmed with hot-stage microscopy and DSC. The absence of eutectic melting in the DSC curves of the labeled α-CD(-SH)s confirmed that neither DLF nor Cou were present in crystalline form. DLF and Cou exhibited sharp melting endotherms at 63.4°C and 208.2°C, respectively (Figure S4). Decomposition of the labeled α-CD(-SH)s occurred above the dyes' melting points and at higher temperatures than for unlabeled α-CD(-SH)s. Therefore, it may be inferred that labeled α-CD(-SH)s exhibit, due to complexation, a higher thermal stability than the single component molecules.

Flow cytometry analyses of these complexes are presented in **Figures 5 A, C, and E**, respectively, for Caco-2, HEK, and MC3T3 cells, while the corresponding calculation of RMFI is shown in **Figures 5B, D, and F**. A shift of fluorescence intensity towards higher values confirmed an enhanced cellular uptake in all tested cells when treated with α-CD-SH, compared to control and cells treated with α-CD (**Figure 5A, C, E**). This was reflected in an increase in RMFI for α-CD-SH samples compared to native α-CDs for all tested cell lines ($p<0.01$). α-CD-SH labeled with DLF showed approximately 20 times higher cellular uptake in Caco-2 cells than native α-CD (**Figure 5 B**). Using coumarin-6 in the same experimental setup led to a 5-fold higher cellular uptake of the thiolated complex. α-CD-SH labeled with DLF (α-CD-SH/DLF) showed 3-fold higher cellular uptake than α-CD, while this difference was approximately 6.5-fold in samples labeled with coumarin-6 for HEK 293 cells (**Figure 5D**).

Similarly, a 14.5-fold increase was obtained for α-CD-SH/DLF and an 11-fold increase for α-CD-SH/Cou in MC3T3 (**Figure 5F**).

In order to better understand the mechanism involved in native and thiolated α-CD cellular uptake, we performed uptake experiments at 4°C to analyze the energy-dependent endocytosis pathway. Most endocytic pathways are energy-dependent processes that can be inhibited at low temperatures (Hsu et al., 2017) since cells consume less ATP at this temperature and active transport is blocked. Here, a dramatic decrease in cellular uptake at 4°C compared with 37°C was observed. Uptake of α-CD labeled with DLF by Caco-2 cells at 4°C was 4-fold lower compared to 37°C. This ratio was approximately 5-fold higher in samples labeled with coumarin-6 (**Figure 5 B**). For HEK 293 cells, uptake was 2.5 times higher in α-CD-SH/DLF, while 7-fold in α-CD-SH/Cou at 4°C (**Figure 5 C and D**). In the MC3T3 cell line, uptake of α-CD labeled with DLF and coumarin-6 was at 4°C 3-fold and 6-fold lower than at 37°C, respectively (**Figure 5 F**).

The decrease in cellular uptake at low temperatures indicates that cells internalize α-CDs via energy-dependent endocytosis. Generally, the uptake of α-CD-SH was on all tested cell lines at 4 °C, also higher than the native one (**Figure 5 B, D, and F**). The results revealed that thiolation significantly increases the cellular uptake of α-CD and that energy-dependent endocytosis is involved in this uptake mechanism.

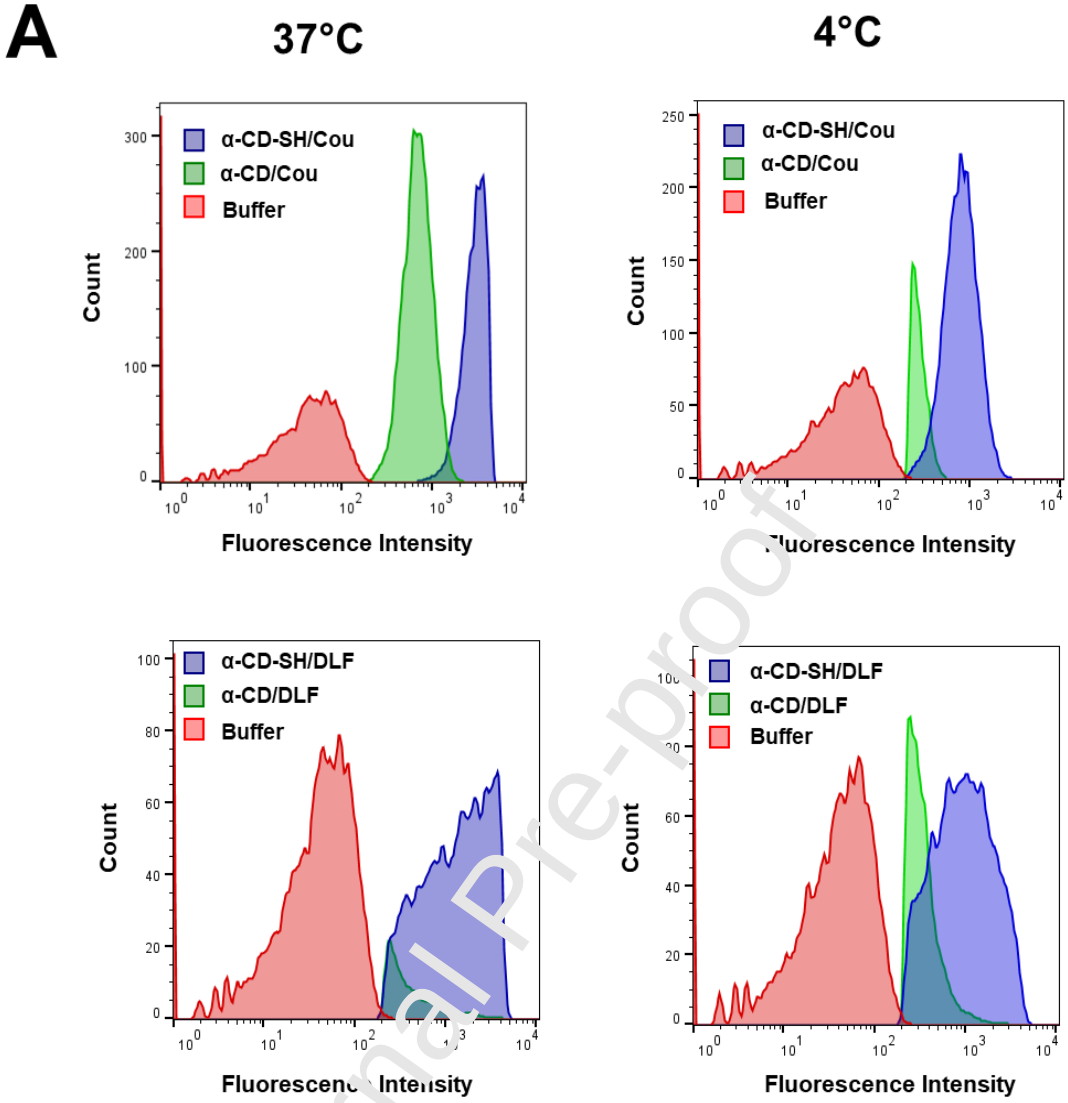

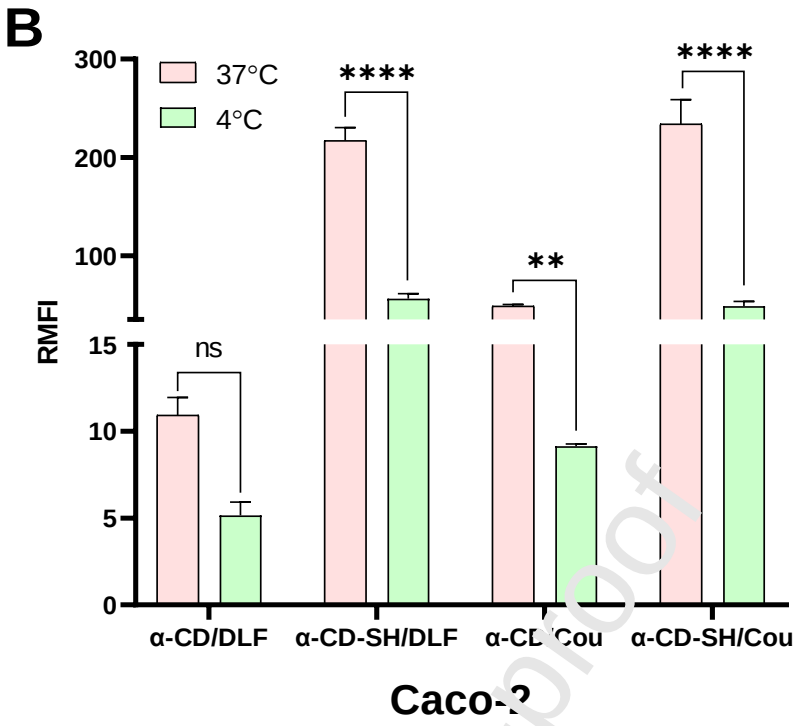

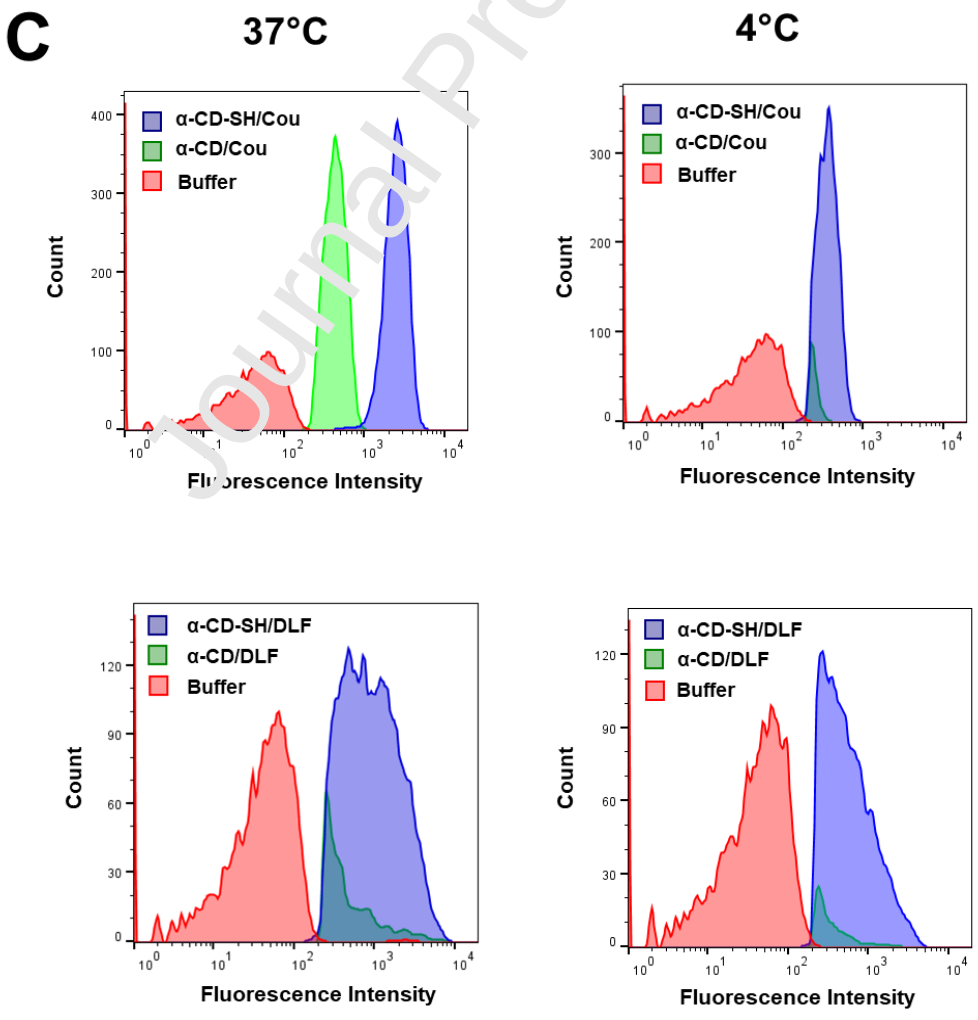

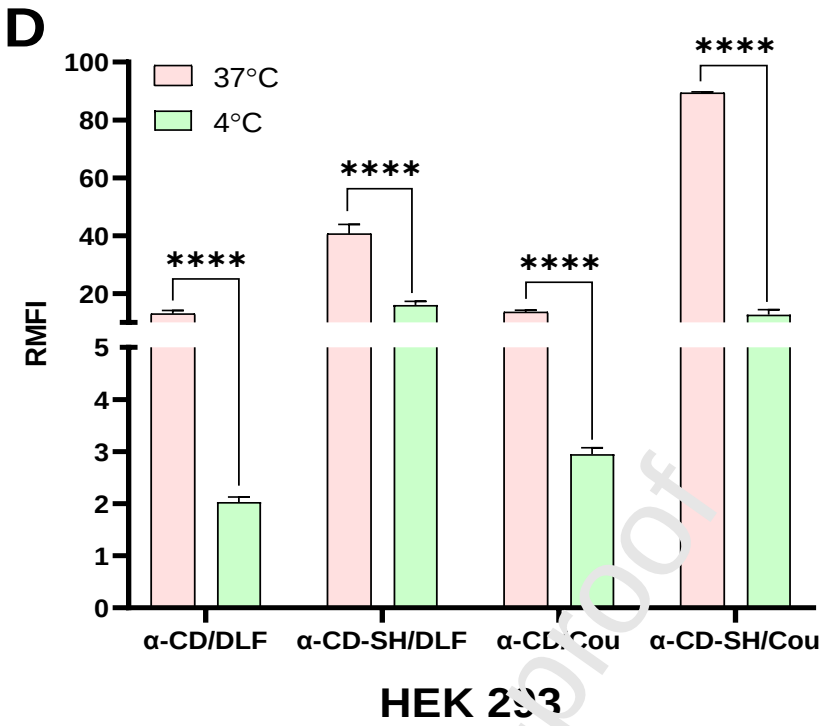

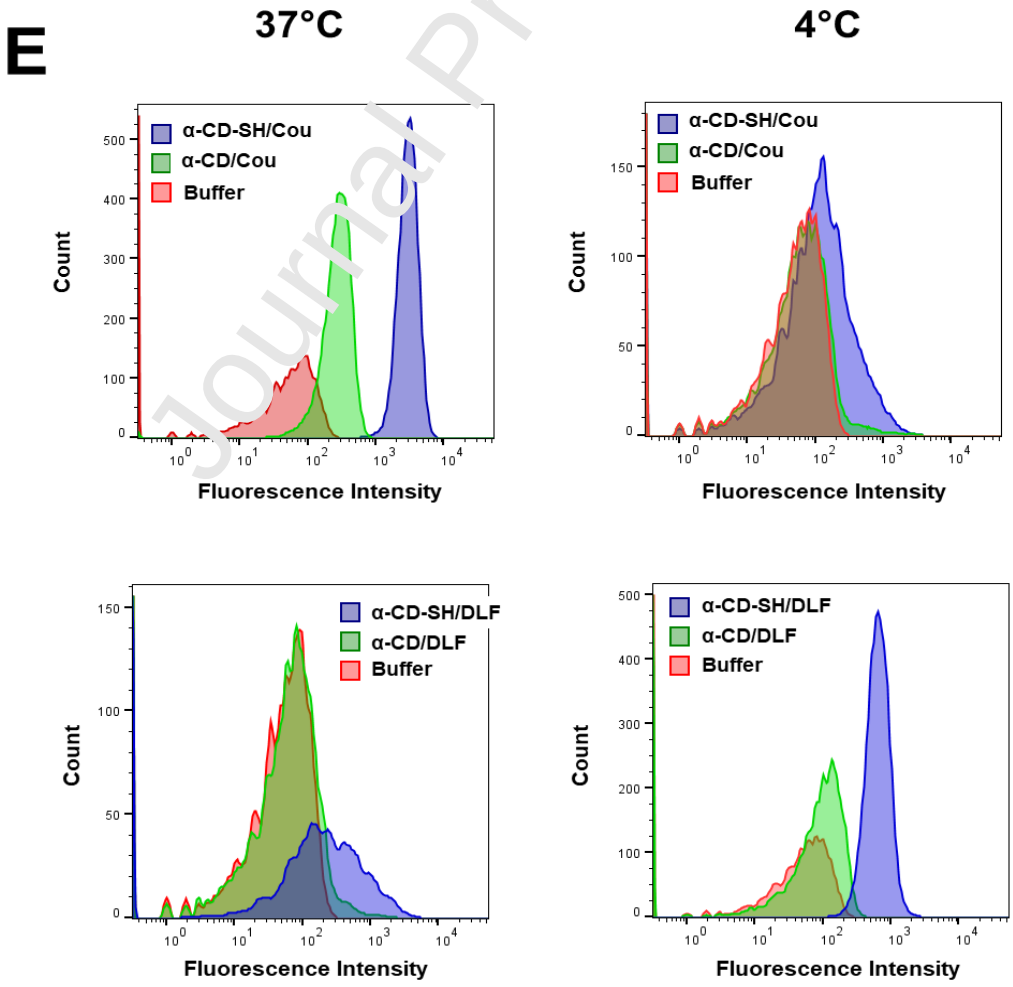

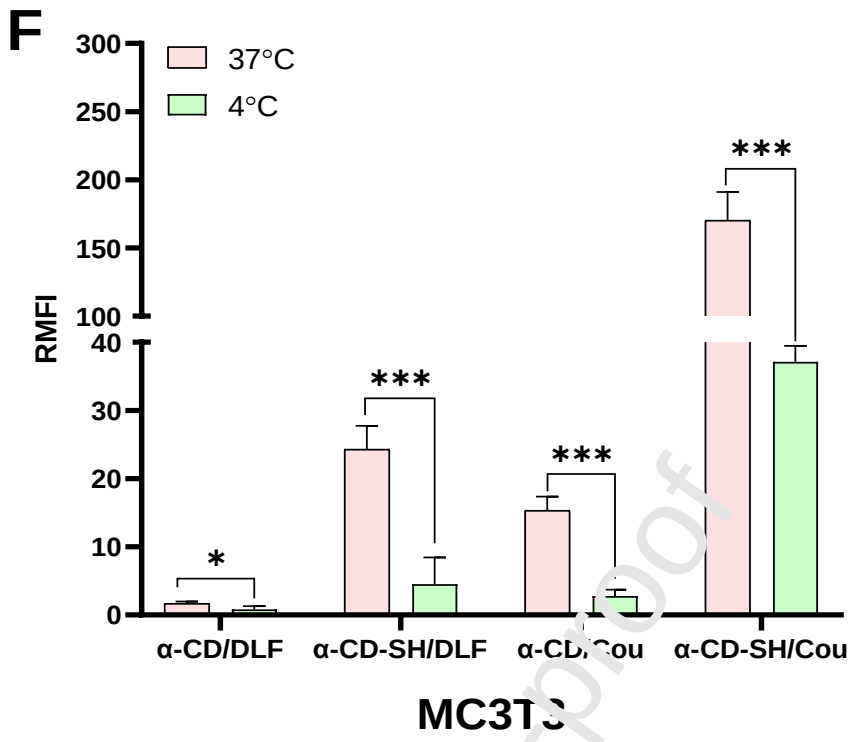

Figure 5. Analysis of cellular uptake of native and thiolated α-CD labeled with DLF and coumarin-6 in Caco-2, HEK 293, and MC3T3 cell lines at 37 °C and 4 °C. Shift in fluorescence intensity and relative mean fluorescence intensity (RMFI) are presented for Caco-2 (A, B), HEK 293 (C, D) and MC3T3 (E, F) cells. *α-CD/DLF: DLF labeled native α-CD, α-CD-SH/DLF: DLF labeled thiolated α-CD, α-CD/Cou: Coumarin-6 labeled native α-CD, α-CD-SH/Cou: Coumarin-6 labeled thiolated α-CD. *p<0.05; ** p<0.005; *** p<0.0005; **** p<0.00005.*

It has been demonstrated in studies using fluorescently labeled CDs that the main internalization pathways of CDs are macropinocytosis and clathrin-dependent endocytosis (Fenyvesi et al., 2014; Plazzo et al., 2012; Réti-Nagy et al., 2015; Rusznyák et al., 2022). However, the cellular uptake of thiolated CDs has not been thoroughly investigated, and thiol-mediated cellular uptake is poorly understood (Laurent et al., 2021). For thiol-mediated cellular uptake,

mechanisms such as endocytosis, fusion, and direct translocation across the plasma membrane to the cytosol have been proposed. Thiol modification increases the cellular delivery efficiency of the carrier system by enabling interactions with cell surface thiols (Cheng et al., 2021). Recently, a thiol-reactive chloride channel CLIC1, an epithelial growth factor receptor EGFR, a transferrin receptor protein-disulfide isomerase, and Ca-activated scramblase TMEM16F proteins have been identified in detail as possible cell surface targets of thiol groups (Laurent et al., 2021). It has been revealed that thiol-modified carrier systems show higher cell permeability-enhancing effects than their non-thiolated counterparts due to thiol-disulfide exchange reactions (Li T & Takeoka S, 2014; Zhang, Qin, Kong, Chen, & Pan, 2019). These findings support the data obtained in our study. Considering the efficacy of thiolation on α-CD on alternative thiol-mediated cellular uptake and endosomal escape, the current strategy can be applied to chemically diverse biomolecules, as well as used to target multiple cell types.

To support flow cytometry results, we examined cellular uptake by confocal microscopy. As shown in **Figure 6**, cells treated with α-CD-SH/DLF exhibit much higher fluorescence compared to native α-CD. This supports the cellular uptake data obtained by flow cytometry. Moreover, in the case of DLF, fluorescence was also found in the nucleus of cells. This coincides with hemolysis experiments, confirmed that thiolation promotes endosomal escape. An additional indication for endosomal escape is the diffuse fluorescence observed in these cells rather than a dotted fluorescence that would indicate endocytosis without endosomal escape. Confocal microscopy results showed furthermore that native and thiolated α-CDs exhibited a significant fluorescence in Caco-2 and HEK cells (**Figure 6A and B**, respectively). In contrast, just α-CD-SH/DLF was taken up by MC3T3 cells (**Figure 6C**).

When comparing confocal images of samples labeled with coumarin-6 with those labeled with DLF, results obtained for thiolated α-CDs were correlated with those of flow cytometry for all cells. I.e., uptake followed the pattern α-CD-SH/Cou = α-CD-SH/DLF for Caco-2 (**Figure 5 B**

compared with **Figure 6 A**), and α-CD-SH/Cou > α-CD-SH/DLF for HEK and MC3T3. (**Figure 5 D** and **E**, compared with **Figures 6 B** and **C**). However, for non-thiolated α-CD, coumarin-6 labeled samples showed increased fluorescence in confocal images (**Figure 6**) compared to flow cytometry results (**Figure 5**). In contrast to DLF, which becomes fluorescent only after enzymatic cleavage of the lauryl ester in the cell, coumarin-6 does not require such an enzymatic activation and can always be detected at λ_{Ex} 457 nm and λ_{Em} 501 nm. Therefore, fluorescence observed in confocal images of α-CD/Cou could be partly attributed to samples that adhere to the surface and do not enter the cell. In flow cytometry analyses, unlike confocal microscopy, this fluorescence is quenched by trypan blue, allowing for discrimination of samples that are taken up from that adsorbed by cells. Trypan blue has been shown to quench fluorescence in close contact with fluorescein isothiocyanate-labeled compounds. According to its physicochemical properties, trypan blue cannot pass through intact membranes of living cells and, therefore, cannot quench intracellular fluorescence (Vranic et al., 2013). Ibrahim et al. revealed that despite washing procedures, nanoparticles that were not taken up into cells were still present in flow cytometry analysis. These free nanoparticles exhibited low forward scattering and high fluorescence due to their small size compared to the cell size. Therefore, they could be tuned to exclude background fluorescence of free nanoparticles in flow cytometry analysis (Ibrahim, Mukhzuddin Bin Mohd Rosli, & Doolaanea, 2020). This comparable exclusion criterion is also used in other studies (Salvati et al., 2018). However, in confocal microscopy studies, it is difficult to distinguish the background originating from fluorescent nanoparticles attached to the cell surface. When dilauryl fluorescein is removed by esterases/lipases in the cell by hydrolysis of lauric acid, fluorescein is released, and fluorescence can be observed at λ_{Ex} 492 nm and λ_{Em} 515 nm (Ge et al., 2007). If fluorescein dilaurate is not hydrolyzed, there is no fluorescence at the indicated wavelengths, and the extracellular DLF does not produce any background signals. This allows for more accurate monitoring of cellular

uptake compared to coumarin-6. Besides being used as a bright and convenient label for the visualization of various delivery systems, coumarin-6 is considered a suitable model of a hydrophobic drug, given its low toxicity (Rivolta et al., 2011). However, in our work, despite all these advantages of coumarin-6, DLF was more advantageous in cellular uptake experiments and showed a correlation between flow cytometry results and confocal microscopy results. The main reason for this difference is that DLF fluoresces when hydrolyzed by cellular esterases/lipases. In confocal microscopy, unlike coumarin-6-labeled CDs, DLF-labeled CDs that adhere to the cell surface and cannot enter the cell do not allow background images.

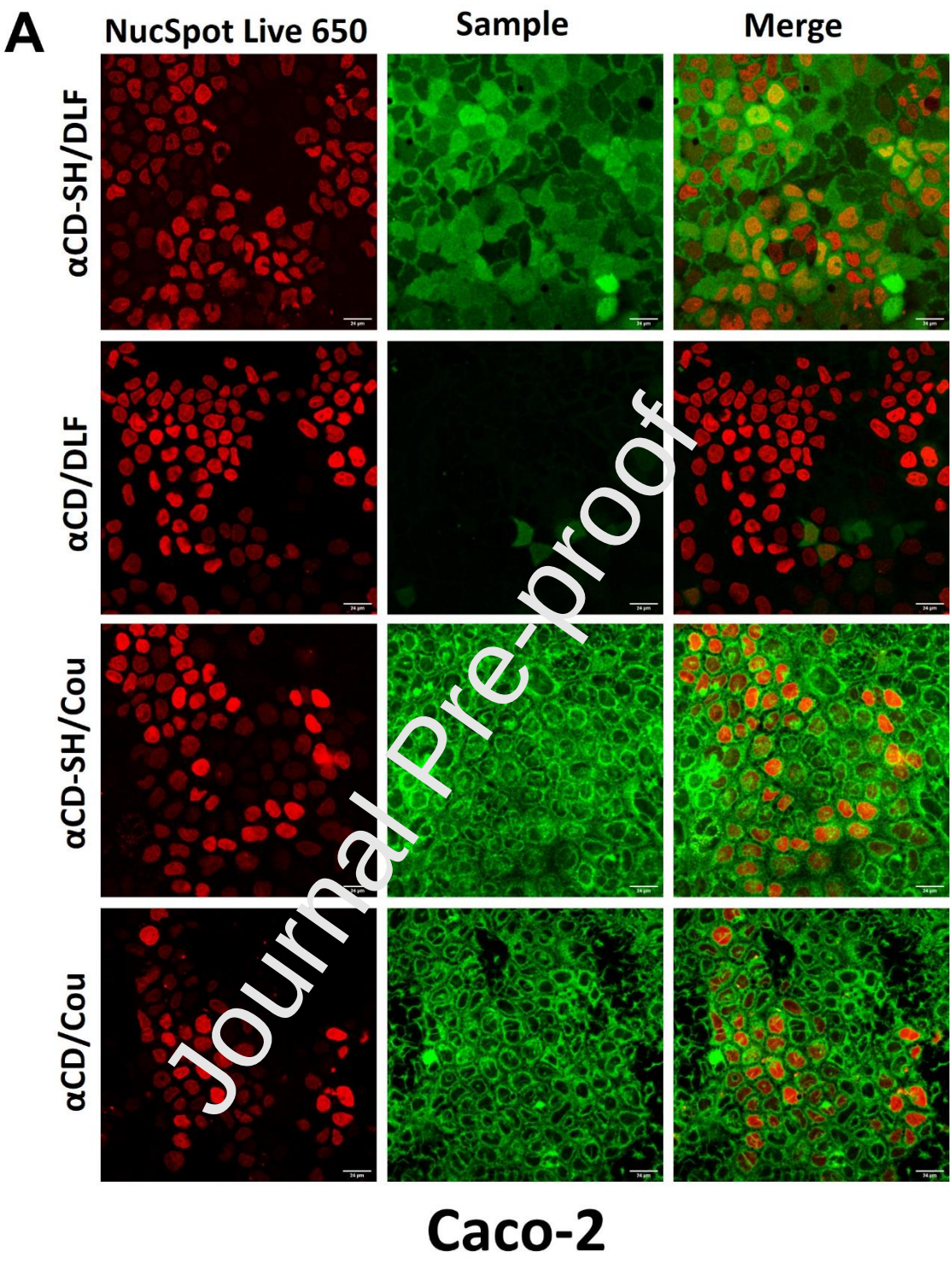

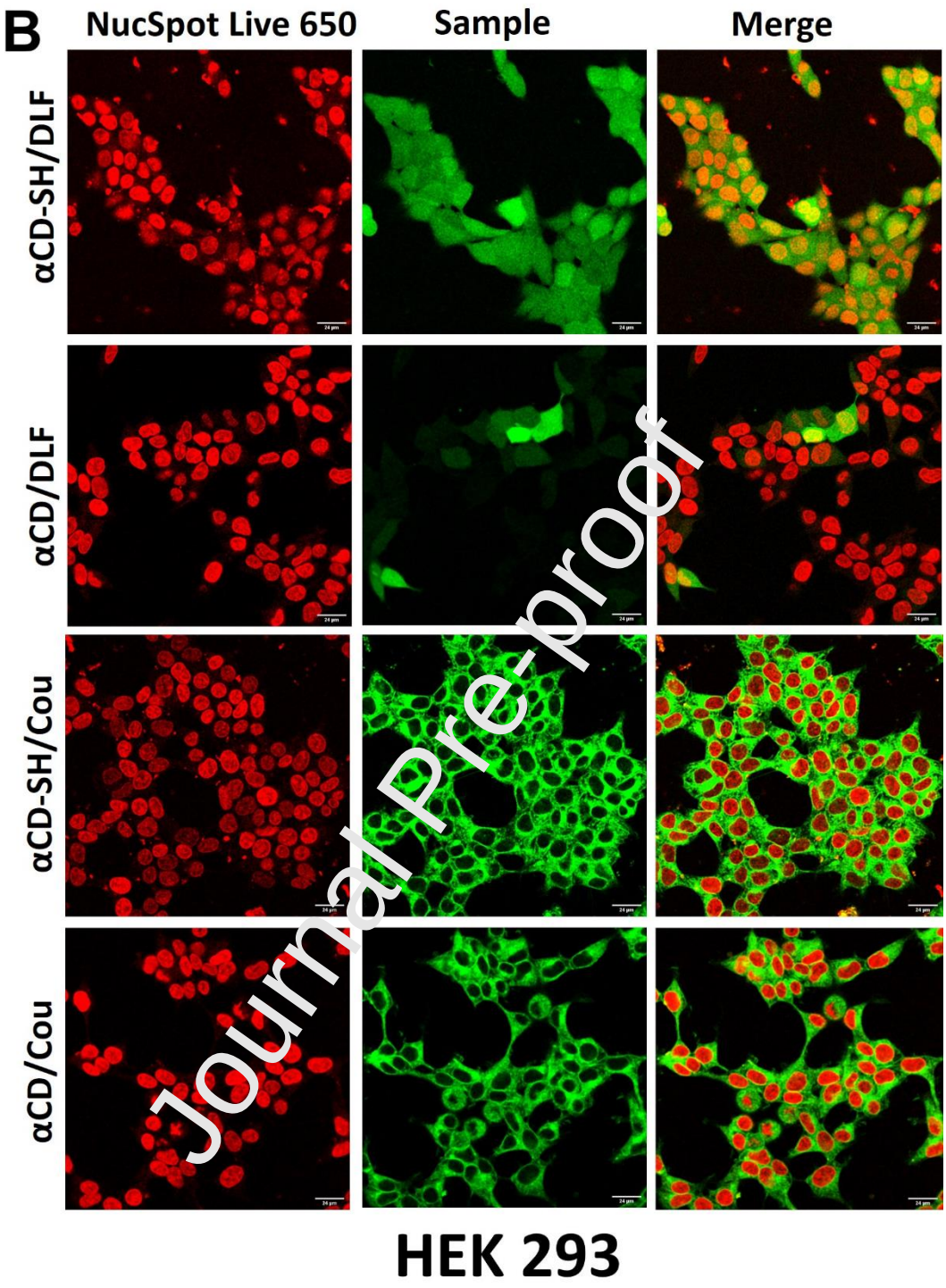

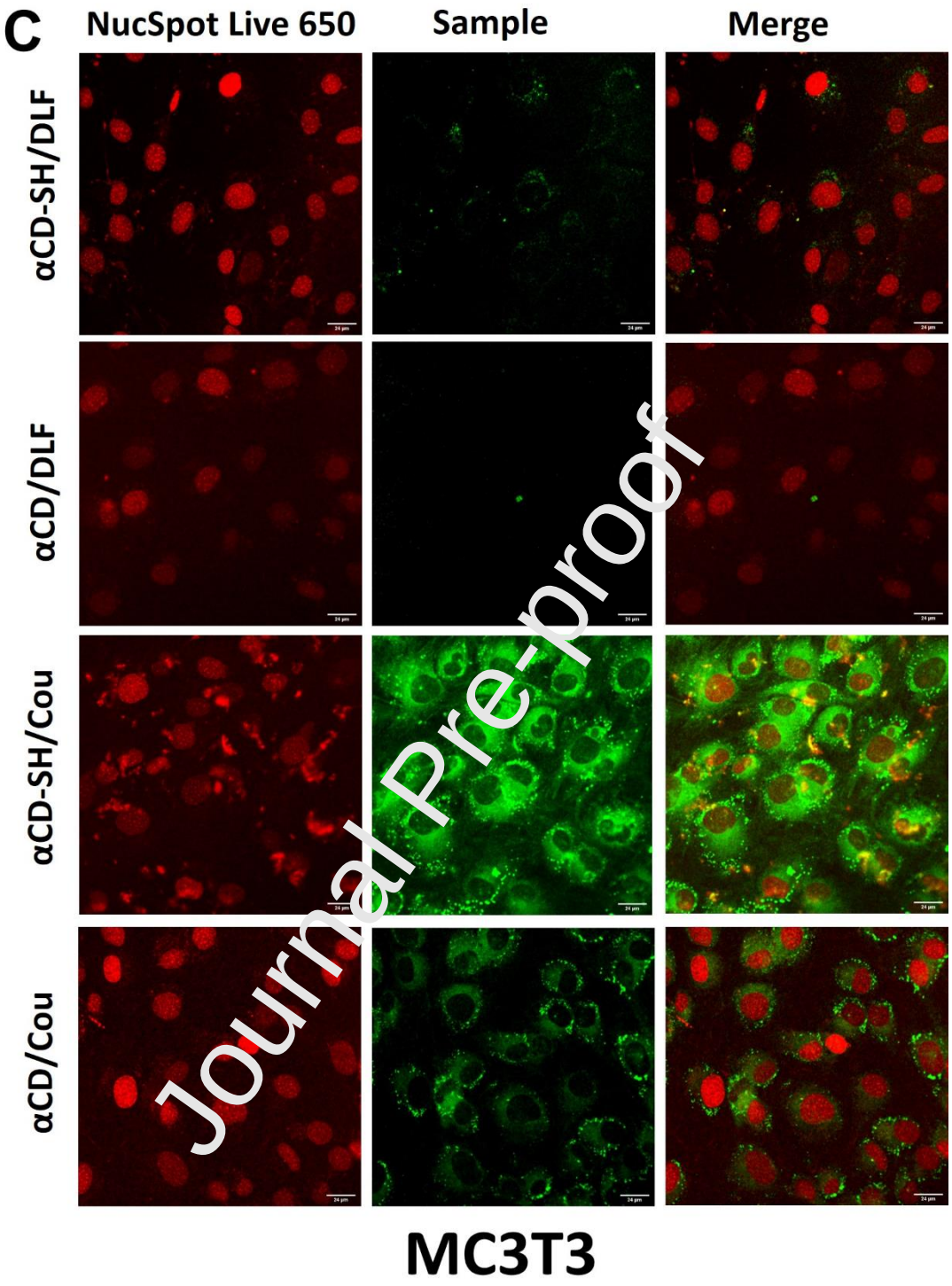

Figure 6. Visualization of cellular uptake using a confocal microscope. (A) Caco-2, (B) HEK 293, (C) MC3T3 cells exposed to fluorescently labeled native and thiolated α-CD for 3 h. The nucleus was stained with NucSpot Live 650. *α-CD/DLF: DLF labeled native α-CD, α-CD-SH/DLF: DLF labeled thiolated α-CD, α-CD/Cou: Coumarin-6 labeled native α-CD, α-CD-SH/Cou: Coumarin-6 labeled thiolated α-CD*

4. CONCLUSION

In this study, we demonstrated the impact of thiol groups on CD-based drug carriers on cellular uptake and endosomal escape for the first time. The formation of thiolated α-CD was confirmed by FT-IR and ^{1}H NMR spectroscopy, and the crystalline state of the materials was identified by PXRD and thermal analysis. Cellular uptake experiments on Caco-2, HEK 293, and MC3T3 cells showed that thiolated α-CD could enter cells at a greater extent than native CD, with uptake driven by energy-dependent endocytosis. The results confirmed the hypothesis that thiolated α-CD increases cellular uptake. Additionally, the hypothesis that endosomal escape is promoted by thiolation was generated and confirmed by confocal microscopy and hemolysis assays. The striking effects of thiol modifications on cellular uptake and endosomal escape in CDs can be used in the pharmaceutical field to deliver hydrophobic drugs into target cells. Therefore, this study will provide strong motivation for the design of α-CD-SH based drug delivery systems in the future.

CrediT authorship contribution statement

Özlem Kaplan, Manuscript writing, correction, proof reading, synthesis, data analyses and interpretation, cellular uptake studies

Martyna Truszkowska, Writing, correction, proof reading, confocal microscopy experiments

Gergely Kali, Writing, correction, proof reading, NMR studies, synthesis, FTIR

Patrick Knoll, Manuscript correction, proof reading, flow cytometry analyses

Mariana Blanco Massani, Writing, correction, proof reading, MC3T3 cellular uptake studies, overall results interpretation.

Doris Elfriede Braun, Analyses, correction, proof reading, DSC, XRD

Andreas Bernkop-Schnürch, Conceptualization, writing, correction, proof reading

Conflicts of interest

The authors confirm that this article content has no conflicts of interest.

Acknowledgments

Özlem Kaplan was supported by Istanbul University between 03 June 2022-29 August 2022 within the scope of Erasmus+ Internship mobility program. Dr. Mariana Blanco Massani acknowledges the support of the European Union's Horizon 2020 Research and Innovation Programme under Marie Skłodowska-Curie IF [NanoBioRS-101025065].

Refereces

Asim, M. H., Ijaz, M., Mahmood, A., Knoll, P., Jalil, A., Arshad, S., & Bernkop-Schnürch, A. (2021). Thiolated cyclodextrins: Mucoadhesive and permeation enhancing excipients for ocular drug delivery. *International Journal of Pharmaceutics,* 599, 120451.

Asim, M. H., Ijaz, M., Rösch, A. C., & Bernkop-Schnürch, A. (2020). Thiolated cyclodextrins: New perspectives for oral excipients. *Coordination Chemistry Reviews,* 420, 213433.

Asim, M. H., Moghadam, A., Ijaz, M., Mahmood, A., Götz, R. X., Matuszczak, B., & Bernkop-Schnürch, A. (2019). S-protected thiolated cyclodextrins as mucoadhesive oligomers for drug delivery. *Journal of Colloid and Interface Science,* 531, 261-268.

Asim, M. H., Nazir, I., Jalil, A., Laffleur, F., Matuszczak, B., & Bernkop-Schnürch, A. (2020). Per-6-Thiolated Cyclodextrins: A Novel Type of Permeation Enhancing Excipients for BCS Class IV Drugs. *ACS Applied Materials & Interfaces,* 12(7), 7942-7950.

Asim, M. H., Nazir, I., Jalil, A., Matuszczak, B., & Bernkop-Schnürch, A. (2020). Tetradeca-thiolated cyclodextrins: Highly mucoadhesive and in-situ gelling oligomers with prolonged mucosal adhesion. *International Journal of Pharmaceutics,* 577, 119040.

Cheng, Y., Pham, A.-T., Kato, T., Lim, B., Moreau, D., López-Andarias, J., . . . Matile, S. (2021). Inhibitors of thiol-mediated uptake. *Chemical Science,* 12(2), 626-631.

Colthup, N. B., Daly, L. H., & Wiberley, S. E. (1990). *CHAPTER 12 - COMPOUNDS CONTAINING BORON, SILICON, PHOSPHORUS, SULFUR, OR HALOGEN*. In N. B. Colthup, L. H. Daly & S. E. Wiberley (Eds.), *Introduction to Infrared and Raman Spectroscopy (Third Edition)* (pp. 355-385). San Diego: Academic Press

Evans, B. C., Nelson, C. E., Yu, S. S., Beavers, K. R., Kim, A. J., Li, H., . . . Duvall, C. L. (2013). Ex vivo red blood cell hemolysis assay for the evaluation of pH-responsive endosomolytic agents for cytosolic delivery of biomacromolecular drugs. *J Vis Exp*(73), e50166.

Fenyvesi, F., Réti-Nagy, K., Bacsó, Z., Gutay-Tóth, Z., Malanga, M., Fenyvesi, É., . . . Bácskay, I. (2014). Fluorescently Labeled Methyl-Beta-Cyclodextrin Enters Intestinal Epithelial Caco-2 Cells by Fluid-Phase Endocytosis. *PLOS ONE*, 9(1), e84856.

Friedl, J. D., Steinbring, C., Zaichik, S., Le, N. N., & Bernkop-Schnürch, A. (2020). Cellular uptake of self-emulsifying drug-delivery systems: polyethylene glycol versus polyglycerol surface. *Nanomedicine (Lond)*, 15(19), 1829-1841.

Fürst, A., Kali, G., Efiana, N. A., Akkın-Dağdeviren, Z. B., Haddadzadegan, S., & Bernkop-Schnürch, A. (2023). Thiolated cyclodextrins: A comparative study of their mucoadhesive properties. *International Journal of Pharmaceutics*, 635, 122719.

Ge, F.-Y., Chen, L.-G., Zhou, X.-L., Pan, H.-Y., Yan, F.-Y., Bai, G.-Y., & Yan, X.-L. (2007). Synthesis and study on hydrolytic properties of fluorescein esters. *Dyes and Pigments*, 72(3), 322-326.

Gérard Yaméogo, J. B., Mazet, R., Wouessidjewe, D., Choisnard, L., Godin-Ribuot, D., Putaux, J.-L., . . . Gèze, A. (2020). Pharmacokinetic study of intravenously administered artemisinin-loaded surface-decorated amphiphilic γ-cyclodextrin nanoparticles. *Materials Science and Engineering: C*, 106, 110281.

Ghosh, P., Das, T., Maity, A., Mondal, S., & Purkayastha, P. (2015). Incorporation of Coumarin 6 in cyclodextrins: microcrystals to lamellar composites. *RSC Advances*, 5(6), 4214-4218.

Gong, X., Liang, Z., Yang, Y., Liu, H., Ji, J., & Fan, Y. (2020). A resazurin-based, nondestructive assay for monitoring cell proliferation during a scaffold-based 3D culture process. *Regenerative Biomaterials*, 7(3), 271-281.

Grassiri, B., Cesari, A., Balzano, F., Migone, C., Kali, G., Bernkop-Schnürch, A., . . . Piras, A. M. (2022). Thiolated 2-Methyl-β-Cyclodextrin as a Mucoadhesive Excipient for Poorly Soluble Drugs: Synthesis and Characterization. *Polymers*, 14(15), 3170.

Grassiri, B., Knoll, P., Fabiano, A., Piras, A. M., Zambito, Y., & Bernkop-Schnürch, A. (2022). Thiolated Hydroxypropyl-β-cyclodextrin: A Potential Multifunctional Excipient for Ocular Drug Delivery. *International Journal of Molecular Sciences*, 23(5), 2612.

Hsu, Y.-H., Hsieh, H.-L., Viswanathan, G., Voon, S. H., Kue, C. S., Saw, W. S., . . . Chung, L. Y. (2017). Multifunctional carbon-coated magnetic sensing graphene oxide-cyclodextrin nanohybrid for potential cancer theranosis. *Journal of Nanoparticle Research*, 19(11), 355.

Ibrahim, W. N., Muizzuddin Bin Mohd Rosli, L., & Doolaanea, A. A. (2020). Formulation, Cellular Uptake and Cytotoxicity of Thymoquinone-Loaded PLGA Nanoparticles in Malignant Melanoma Cancer Cells. *Int J Nanomedicine*, 15, 8059-8074.

Ijaz, M., Matuszczak, B., Rahmat, D., Mahmood, A., Bonengel, S., Hussain, S., . . . Bernkop-Schnürch, A. (2015). Synthesis and characterization of thiolated β-cyclodextrin as a novel mucoadhesive excipient for intra-oral drug delivery. *Carbohydrate Polymers*, 132, 187-195.

Jacob, S., & Nair, A. B. (2018). Cyclodextrin complexes: Perspective from drug delivery and formulation. *Drug Development Research*, 79(5), 201-217.

Jicsinszky, L. (2019). Some comments on the Cyclodextrin solubilities. *MOJ Biorg Org Chem*, 3(1), 11-13.

Kali, G., Haddadzadegan, S., Laffleur, F., & Bernkop-Schnürch, A. (2023). Per-thiolated cyclodextrins: Nanosized drug carriers providing a prolonged gastrointestinal residence time. *Carbohydrate Polymers*, 300, 120275.

Kanjilal, P., Dutta, K., & Thayumanavan, S. (2022). Thiol-Disulfide Exchange as a Route for Endosomal Escape of Polymeric Nanoparticles. *Angewandte Chemie International Edition*, 61(37), e202209227.

Laquintana, V., Asim, M. H., Lopedota, A., Cutrignelli, A., Lopalco, A., Franco, M., . . . Denora, N. (2019). Thiolated hydroxypropyl-β-cyclodextrin as mucoadhesive excipient for oral delivery of budesonide in liquid paediatric formulation. *International Journal of Pharmaceutics*, 572, 118820.

Laurent, Q., Martinent, R., Lim, B., Pham, A.-T., Kato, T., López-Andarias, J., . . . Matile, S. (2021). Thiol-Mediated Uptake. *JACS Au*, 1(6), 710-728.

Lázaro, C. M., de Oliveira, C. C., Gambero, A., Rocha, T., Cereda, C. M. S., de Araújo, D. R., & Tofoli, G. R. (2020). Evaluation of Budesonide–Hydroxypropyl-β-Cyclodextrin Inclusion Complex in Thermoreversible Gels for Ulcerative Colitis. *Digestive Diseases and Sciences*, 65(11), 3297-3304.

Li, B.-L., Zhang, J., Jin, W., Chen, X.-Y., Yang, J.-M., Chi, S.-M., . . . Zhao, Y. (2022). Oral administration of pH-responsive polyamine modified cyclodextrin nanoparticles for controlled release of anti-tumor drugs. *Reactive and Functional Polymers*, 172, 105175.

Li T, & Takeoka S. (2014). Enhanced cellular uptake of maleimide-modified liposomes via thiol-mediated transport *Int J Nanomedicine*, 9(1), 2849-2861.

Loftsson, T., Jarho, P., Másson, M., & Järvinen, T. (2005). Cyclodextrins in drug delivery. *Expert Opinion on Drug Delivery*, 2(2), 335-351.

Londhe, V., & Shirsat, R. (2018). Formulation and Characterization of Fast-Dissolving Sublingual Film of Iloperidone Using Box–Behnken Design for Enhancement of Oral Bioavailability. *AAPS PharmSciTech*, 19(3), 1392-1400.

Loretz, B., Thaler, M., & Bernkop-Schnürch, A. (2007). Role of Sulfhydryl Groups in Transfection? A Case Study with Chitosan−NAC Nanoparticles. *Bioconjugate Chemistry*, 18(4), 1028-1035.

Manor, P. C., & Saenger, W. (1974). Topography of cyclodextrin inclusion complexes. III. Crystal and molecular structure of cyclohexaamylose hexahydrate, the water dimer inclusion complex. *Journal of the American Chemical Society*, 96(11), 3630-3639.

Mirankó, M., Tóth, J., Bartos, C., Ambrus, R., & Feczkó, T. (2023). Nano-Spray-Dried Levocetirizine Dihydrochloride with Mucoadhesive Carriers and Cyclodextrins for Nasal Administration. *Pharmaceutics*, 15(2), 317.

Oktay, A. N., Celebi, N., Ilbasmis-Tamer, S., & Kaplanoğlu, G. T. (2023). Cyclodextrin-based nanogel of flurbiprofen for dermal application: In vitro studies and in vivo skin irritation evaluation. *Journal of Drug Delivery Science and Technology*, 79, 104012.

Pei, D., & Buyanova, M. (2019). Overcoming Endosomal Entrapment in Drug Delivery. *Bioconjug Chem*, 30(2), 273-283.

Plazzo, A. P., Höfer, C. T., Jicsinszky, L., Fenyvesi, É., Szente, L., Schiller, J., . . . Müller, P. (2012). Uptake of a fluorescent methyl-β-cyclodextrin via clathrin-dependent endocytosis. *Chemistry and Physics of Lipids*, 165(5), 505-511.

Poulson, B. G., Alsulami, Q. A., Sharfalddin, A., El Agammy, E. F., Mouffouk, F., Emwas, A.-H., . . . Jaremko, M. (2022). Cyclodextrins: Structural, Chemical, and Physical Properties, and Applications. *Polysaccharides*, 3(1), 1-31.

Réti-Nagy, K., Malanga, M., Fenyvesi, É., Szente, L., Vámosi, G., Váradi, J., . . . Fenyvesi, F. (2015). Endocytosis of fluorescent cyclodextrins by intestinal Caco-2 cells and its role in paclitaxel drug delivery. *International Journal of Pharmaceutics*, 496(2), 509-517.

Rivolta, I., Panariti, A., Lettiero, B., Sesana, S., Gasco, P., Gasco, M. R., . . . Miserocchi, G. (2011). Cellular uptake of coumarin-6 as a model drug loaded in solid lipid nanoparticles. *J Physiol Pharmacol*, 62(1), 45-53.

Rusznyák, Á., Palicskó, M., Malanga, M., Fenyvesi, É., Szente, L., Váradi, J., . . . Fenyvesi, F. (2022). Cellular Effects of Cyclodextrins: Studies on HeLa Cells. *Molecules*, 27(5).

Sahoo, D., Bandaru, R., Samal, S. K., Naik, R., Kumar, P., Kesharwani, P., & Dandela, R. (2021). *Chapter 9 - Oral drug delivery of nanomedicine*. In P. Kesharwani, S. Taurin & K. Greish (Eds.), *Theory and Applications of Nonparenteral Nanomedicines* (pp. 181-207): Academic Press

Salvati, A., Nelissen, I., Haase, A., Åberg, C., Moya, S., Jacobs, A., . . . Dawson, K. A. (2018). Quantitative measurement of nanoparticle uptake by flow cytometry illustrated by an interlaboratory comparison of the uptake of labelled polystyrene nanoparticles. *NanoImpact*, 9, 42-50.

Saouane, S., & Fabbiani, F. P. A. (2016). Structural Elucidation of α-Cyclodextrin-Succinic Acid Pseudo Dodecahydrate: Expanding the Packing Types of α-Cyclodextrin Inclusion Complexes. *Crystals*, 6(1), 2.

Srivastava, G. K., Reinoso, R., Singh, A. K., Fernandez-Bueno, I., Hileeto, D., Martino, M., . . . Pastor, J. C. (2011). Trypan Blue staining method for quenching the

autofluorescence of RPE cells for improving protein expression analysis. *Exp Eye Res*, 93(6), 956-962.

Syed Haroon, K., Mehreen, B., Sajid, A., Tauqeer Hussain, M., & Ikram Ullah, K. (2019). *Effect of Cyclodextrin Derivatization on Solubility and Efficacy of Drugs*. In K. Selcan (Ed.), *Colloid Science in Pharmaceutical Nanotechnology* (p. Ch. 7). Rijeka: IntechOpen

Taylor, R., & Wood, P. A. (2019). A Million Crystal Structures: The Whole Is Greater than the Sum of Its Parts. *Chemical Reviews*, 119(16), 9427-9477.

Topuz, F. (2022). Rapid Sublingual Delivery of Piroxicam from Electrospun Cyclodextrin Inclusion Complex Nanofibers. *ACS Omega*, 7(39), 35083-35091.

Torres, A. G., & Gait, M. J. (2012). Exploiting cell surface thiols to enhance cellular uptake. *Trends Biotechnol*, 30(4), 185-190.

Veider, F., Akkuş-Dağdeviren, Z. B., Knoll, P., & Bernkop-Schnürch, A. (2022). Design of nanostructured lipid carriers and solid lipid nanoparticles for enhanced cellular uptake. *International Journal of Pharmaceutics*, 624, 122014.

Vranic, S., Boggetto, N., Contreras-Sandoval, A. M., Mornet, S., Reinhardt, N., Marano, F., . . . Boland, S. (2013). Deciphering the mechanisms of cellular uptake of engineered nanoparticles by accurate evaluation of internalization using imaging flow cytometry. *Particle and Fibre Toxicology*, 10(1), 2.

Wang, L.-L., Zheng, W.-S., Chen, S.-H., Han, Y.-X., & Jiang, J.-D. (2016). Development of rectal delivered thermo-reversible gelling film encapsulating a 5-fluorouracil hydroxypropyl-β-cyclodextrin complex. *Carbohydrate Polymers*, 137, 9-18.

Wang, Q., Zhang, A., Zhu, L., Yang, X., Fang, G., & Tang, B. (2023). Cyclodextrin-based ocular drug delivery systems: A comprehensive review. *Coordination Chemistry Reviews*, 476, 214919.

Zhang, R., Qin, X., Kong, F., Chen, P., & Pan, G. (2019). Improving cellular uptake of therapeutic entities through interaction with components of cell membrane. *Drug Delivery*, 26(1), 328-342.

Declaration of interests

☒The authors declare that they have no known competing financial interests or personal relationships that could have appeared to influence the work reported in this paper.

☐The authors declare the following financial interests/personal relationships which may be considered as potential competing interests: